PERGAMON

International Journal of Heat and Mass Transfer 45 (2002)1185–1195

International Journal of HEAT and MASS TRANSFER

www.elsevier.com/locate/ijhmt

Stability analysis of natural convection in porous cavities through integral transforms

L.S. de B. Alves [a], R.M. Cotta [a,*], J. Pontes [b]

[a] *Laboratório de Transmissão e Tecnologia do Calor (LTTC), Programa de Engenharia Mecânica, EE, COPPE, Universidade Federal do Rio de Janeiro, Cidade Universitária, Cx. Postal 68503, Rio de Janeiro, RJ, 21945-970, Brazil*

[b] *Programa de Engenharia Metalúrgica e de Materiais, EE, COPPE, Universidade Federal do Rio de Janeiro, Cidade Universitária, Cx. Postal 68503, Rio de Janeiro, RJ, 21945-970, Brazil*

Received 27 December 2000; received in revised form 6 July 2001

Abstract

The onset of convection and chaos related to natural convection inside a porous cavity heated from below is investigated using the generalized integral transform technique (GITT). This eigenfunction expansion approach generates an ordinary differential system that is adequately truncated in order to be handled by linear stability analysis (LSA) as well as in full nonlinear form through the *Mathematica* software system built-in solvers. Lorenz's system is generated from the transformed equations by using the steady-state solution to scale the potentials. Systems with higher truncation orders are solved in order to obtain more accurate results for the Rayleigh number at onset of convection, and the influence of aspect ratio and Rayleigh number on the cell pattern transition from n to $n+2$ cells ($n = 1, 3, 5, \ldots$) is analyzed from both local and average Nusselt number behaviors. The qualitative dependence of the Rayleigh number at onset of chaos on the transient behavior and aspect ratio is presented for a low dimensional system (Lorenz equations) and its convergence behavior for increasing expansion orders is investigated. © 2002 Published by Elsevier Science Ltd.

1. Introduction

Transport phenomenon in porous media represents an important segment of the heat and mass transfer field and have a variety of applications in engineering. The effect of free convection as a result of the gravitational body force is of particular interest from both practical and theoretical points of view. Engineering applications include among others thermal insulation, radioactive waste disposal, solar energy collectors and geothermal energy analysis. Other applications of the porous medium modeling are discussed by Kakaç et al. [1] and more recently by Kaviany [2].

The present work is concerned with the stability analysis of transient natural convection within a two-dimensional porous cavity heated from below, based on a modified Darcy law that includes the velocity time derivative [3,4]. While steady-state behaviors have been almost fully determined and understood, a substantial amount of research is yet to be undertaken in the analysis of transient nonlinear phenomenon related to natural convection within porous media.

Within the last two decades, the ideas in the so-called generalized integral transform technique (GITT) [5–7] were progressively advanced towards the establishment of an alternative hybrid numerical–analytical approach, based on the formal analytical principles in the classical integral transform method [8], for the solution of a priori nontransformable diffusion and convection–diffusion problems. In the last few years, the analytical steps inherent in the integral transformation procedure were markedly improved by packages that allow for mixed symbolic and numerical computations such as the *Mathematica* system [9,10].

* Corresponding author. Tel.: +55-21-562-8368; fax: +55-21-290-6626.

E-mail address: cotta@serv.com.ufrj.br (R.M. Cotta).

0017-9310/02/$ - see front matter © 2002 Published by Elsevier Science Ltd.
PII: S0017-9310(01)00231-9

Nomenclature

A, B, C	matrix coefficients
c_p	specific heat (J/kg K)
D	matrix coefficient
Da	Darcy number ($= \kappa/l^2$)
E_i	energy input
E_o	energy output
f, f^*	vector coefficients
g	gravity (m/s^2)
h	height of the porous cavity (m)
H	aspect ratio, equals ($= h/l$)
k_e	effective thermal conductivity of the porous medium (W/m K)
l	length of the porous cavity (m)
M	number of terms in the temperature expansion
n	number of cell structures
N	number of terms in the stream function expansion
Nt	total number of equations ($Nt = N + M$)
Nu	local Nusselt number
Nu_{av}	averaged Nusselt number
Nu_{loc}	steady-state local Nusselt number
p_1, p_2, p_3	Lorenz constants
Pr	Prandtl number ($= v(\rho c_p)_e/k_e$)
Ra	Rayleigh number ($= g\beta(\rho c_p)_f \Delta T l \kappa / v k_e$)
Ra_{cond}	critical conduction Rayleigh number
Ra_{conv}	critical convection Rayleigh number
Ra'	scaled Rayleigh number ($= Ra/\pi^2$)
t	re-scaled dimensionless time
T	temperature (K)
ΔT	temperature difference ($= T_h - T_c$) (K)
T_c	cold wall temperature (K)
T_h	hot wall temperature (K)
U, V	dimensionless velocity components ($= u(\rho c_p)_f l/k_m$, $v(\rho c_p)_f l/k_m$)
X	dimensionless vertical coordinate ($= x/l$)
Y_1, Y_2, Y_3	Lorenz potentials
Z	dimensionless horizontal coordinate ($= z/l$)

Greek symbols

α_i	stream function eigenvalue in X-direction
β	isobaric coefficient of thermal expansion of fluid (K^{-1})
β_j	stream function eigenvalue in Z-direction
γ_m	temperature eigenvalue in X-direction
θ	dimensionless temperature ($= (T - T_c)/(T_h - T_c)$)
Θ	dimensionless filtered temperature ($= \theta - X$)
$\tilde{\tilde{\theta}}_{m,n}$	dimensionless transformed temperature
κ	permeability of porous medium (m^2)
λ_n	temperature eigenvalue in Z-direction
v	kinematic viscosity of fluid (m^2/s)
ρ	density (kg/m^3)
τ	dimensionless time ($= tk_m/(\rho C_p)_e l^2$)
Φ	porosity
χ	re-scaled coefficient ($= \phi Pr/Da$)
ψ	dimensionless stream function
$\tilde{\psi}_{i,j}$	dimensionless transformed stream function
Γ, Γ^*	temperature eigenfunctions
Φ, Φ^*	stream function eigenfunctions

Subscripts

av	averaged parameter
c	related to cold wall
e	related to effective property
f	related to fluid property
h	related to hot wall
i, j, k	stream function expansion indices
m, n, o	temperature expansion indices

In the present study, the integral transformation procedure generates an ordinary differential system of equations, which is adequately truncated in order to generate Lorenz equations, and other low dimensional systems, generally employed in linear stability analysis (LSA) [11]. Thereafter, systems with higher truncation orders are generated and a more accurate correlation for the Rayleigh number at onset of convection [12–14] as a function of the aspect ratio is obtained and compared with the results obtained from a direct numerical solution of the full nonlinear system. The influence of the aspect ratio on the cell pattern transition into multiple cells is observed through the steady-state Nusselt number behavior. This transition is also governed by the Rayleigh number and its influence is observed through the steady-state local Nusselt number behavior.

The qualitative behavior of the Rayleigh number at onset of chaos is investigated using a correlation obtained from applying LSA to Lorenz system [3]. This critical parameter behavior, as the truncation order of the nonlinear ordinary differential system is increased, is shown for a specific case and ideas to improve its convergence behavior are discussed.

2. Problem formulation

Consider a two-dimensional fluid saturated porous layer enclosed by two isothermal horizontal walls at temperatures T_h and T_c, $T_h \geqslant T_c$, and two adiabatic vertical walls as presented in Fig. 1, with the walls of the cavity assumed to be impermeable. In the porous

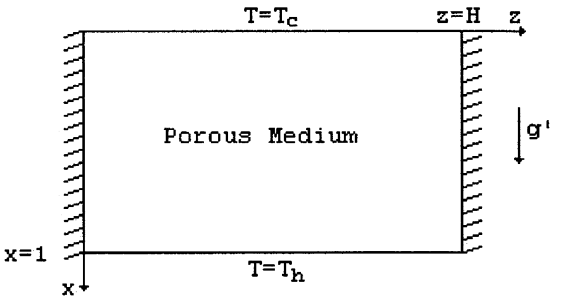

Fig. 1. Representation of two-dimensional horizontal cavity filled with porous material.

medium, Darcy law, modified to include the time derivative term, is assumed to hold, and the fluid is assumed to be Newtonian and the flow to be within Boussinesq approximation limits.

With these assumptions, the dimensionless conservation equations for momentum and energy, transformed to the stream function formulation, for a two-dimensional transient flow in an isotropic porous medium, are [3,4]:

$$\frac{1}{\chi}\frac{\partial}{\partial\tau}\left(\frac{\partial^2\psi}{\partial X^2}+\frac{\partial^2\psi}{\partial Z^2}\right)+\frac{\partial^2\psi}{\partial X^2}+\frac{\partial^2\psi}{\partial Z^2}=-Ra\frac{\partial\theta}{\partial Z}, \tag{1}$$

$$\frac{\partial\theta}{\partial\tau}+\frac{\partial\psi}{\partial Z}\frac{\partial\theta}{\partial X}-\frac{\partial\psi}{\partial X}\frac{\partial\theta}{\partial Z}=\frac{\partial^2\theta}{\partial X^2}+\frac{\partial^2\theta}{\partial Z^2}. \tag{2}$$

The related hydrodynamic and thermal boundary conditions are

$$\psi=0,\ \theta=0 \quad \text{at } X=0, \tag{3}$$

$$\psi=0,\ \theta=1 \quad \text{at } X=1, \tag{4}$$

$$\psi=0,\ \frac{\partial\theta}{\partial Z}=0 \quad \text{at } Z=0, \tag{5}$$

$$\psi=0,\ \frac{\partial\theta}{\partial Z}=0 \quad \text{at } Z=H. \tag{6}$$

The stream function and temperature initial conditions are

$$\psi=\psi_0 \quad \text{at } \tau=0, \tag{7}$$

$$\theta=\theta_0 \quad \text{at } \tau=0, \tag{8}$$

where the stream function distribution is defined from

$$U=\frac{\partial\psi}{\partial Z},\quad V=-\frac{\partial\psi}{\partial X} \tag{9}$$

and the dimensionless parameters used are

$$Pr=\frac{v(\rho c_p)_e}{k_e},\quad Da=\frac{\kappa}{l^2},\quad \chi=\phi\frac{Pr}{Da},$$
$$H=\frac{h}{l}\quad\text{and}\quad Ra=\frac{g\beta(\rho c_p)_f\Delta Tl\kappa}{vk_e}. \tag{10}$$

3. Transformed equations

Following the formalism in the integral transform approach, we choose auxiliary eigenvalue problems for the stream function in the X- and Z-directions, respectively,

$$\frac{d^2\Phi_i(X)}{dX^2}+\gamma_i^2\Phi_i(X)=0,\quad 0\leqslant X\leqslant 1, \tag{11}$$

$$\Phi_i(0)=0,\ \Phi_i(1)=0,\quad i=1,2,\ldots, \tag{12}$$

$$\frac{d^2\Phi_j^*(Z)}{dZ^2}+\lambda_j^2\Phi_j^*(Z)=0,\quad 0\leqslant Z\leqslant H, \tag{13}$$

$$\Phi_j^*(0)=0,\ \Phi_j^*(H)=0,\quad j=1,2,\ldots, \tag{14}$$

where the associated normalized eigenfunctions and eigenvalues are

$$\Phi_i(X)=\sqrt{2}\sin(\gamma_i X),\quad \gamma_i=i\pi, \tag{15}$$

$$\Phi_j^*(Z)=\sqrt{\frac{2}{H}}\sin(\lambda_j Z),\quad \lambda_j=\frac{j\pi}{H}. \tag{16}$$

Following the same procedure, the auxiliary eigenvalue problems for temperature in the X- and Z-directions are

$$\frac{d^2\Gamma_m(X)}{dX^2}+\alpha_m^2\Gamma_m(X)=0,\quad 0\leqslant X\leqslant 1, \tag{17}$$

$$\Gamma_m(0)=0,\ \Gamma_m(1)=0,\quad m=1,2,\ldots, \tag{18}$$

$$\frac{d^2\Gamma_n^*(Z)}{dZ^2}+\beta_n^2\Gamma_n^*(Z)=0,\quad 0\leqslant Z\leqslant H, \tag{19}$$

$$\left.\frac{d\Gamma_n^*(Z)}{dZ}\right|_{Z=0}=0,\ \left.\frac{d\Gamma_n^*(Z)}{dZ}\right|_{Z=H}=0,\quad n=0,1,2,\ldots, \tag{20}$$

where the associated normalized eigenfunctions and eigenvalues are

$$\Gamma_m(X)=\sqrt{2}\sin(\alpha_m X),\quad \alpha_m=m\pi, \tag{21}$$

$$\Gamma_0^*(Z)=\frac{1}{\sqrt{H}},\quad \Gamma_n^*(Z)=\sqrt{\frac{2}{H}}\cos(\beta_n Z),\quad \beta_n=\frac{n\pi}{H}. \tag{22}$$

The eigenvalue problems (11)–(16) and (17)–(22) are of the Sturm–Liouville type and allow definition of the following integral transform pairs:

$$\bar{\psi}_i(Z,\tau)=\int_0^1\Phi_i(X)\psi(X,Z,\tau)\,dX \quad \text{(transform in } X\text{-direction)}, \tag{23}$$

$$\bar{\tilde{\psi}}_{i,j}(\tau)=\int_0^H\Phi_j^*(Z)\bar{\psi}_i(Z,\tau)\,dZ \quad \text{(transform in } Z\text{-direction)}, \tag{24}$$

$$\psi(X,Z,\tau)=\sum_{i=1}^{\infty}\sum_{j=1}^{\infty}\Phi_i(X)\Phi_j^*(Z)\tilde{\bar{\psi}}_{i,j}(\tau)\quad\text{(inverse)},\tag{25}$$

$$\bar{\Theta}_m(Z,\tau)=\int_0^1\Gamma_m(X)\Theta(X,Z,\tau)\,\mathrm{d}X\quad\text{(transform in } X\text{-direction)},\tag{26}$$

$$\tilde{\bar{\Theta}}_{m,n}(\tau)=\int_0^H\Gamma_n^*(Z)\bar{\Theta}_m(Z,\tau)\,\mathrm{d}Z\quad\text{(transform in } Z\text{-direction)},\tag{27}$$

$$\theta(X,Z,\tau)=X+\sum_{m=1}^{\infty}\sum_{n=0}^{\infty}\Gamma_m(X)\Gamma_n^*(Z)\tilde{\bar{\Theta}}_{m,n}(\tau)\quad\text{(inverse)},\tag{28}$$

where a filtering solution was employed to make the temperature boundary conditions homogeneous. Applying the principles of the generalized integral transform technique [5,7] to Eqs. (1)–(6), we obtain the transformed equations shown below:

$$\frac{\mathrm{d}\tilde{\bar{\psi}}_{i,j}(\tau)}{\mathrm{d}\tau}=\chi\left(\frac{Ra}{(\gamma_i^2+\lambda_j^2)}\sum_{m=1}^{\infty}\sum_{n=0}^{\infty}A_{i,j,m,n}\tilde{\bar{\Theta}}_{m,n}(\tau)-\tilde{\bar{\psi}}_{i,j}(\tau)\right),\tag{29}$$

$$\begin{aligned}\frac{\mathrm{d}\tilde{\bar{\Theta}}_{m,n}(\tau)}{d\tau}=&-\sum_{i=1}^{\infty}\sum_{j=1}^{\infty}B_{m,n,i,j}\tilde{\bar{\psi}}_{i,j}(\tau)\\&-\sum_{i=1}^{\infty}\sum_{j=1}^{\infty}\sum_{o=1}^{\infty}\sum_{p=0}^{\infty}C_{m,n,i,j,o,p}\tilde{\bar{\psi}}_{i,j}(\tau)\tilde{\bar{\Theta}}_{o,p}(\tau)\\&+\sum_{i=1}^{\infty}\sum_{j=1}^{\infty}\sum_{o=1}^{\infty}\sum_{p=0}^{\infty}D_{m,n,i,j,o,p}\tilde{\bar{\psi}}_{i,j}(\tau)\tilde{\bar{\Theta}}_{o,p}(\tau)\\&-(\alpha_m^2+\beta_n^2)\tilde{\bar{\Theta}}_{m,n}(\tau)\end{aligned}\tag{30}$$

and the integral transformation of the initial conditions (7) and (8) yields

$$\tilde{\bar{\psi}}_{i,j}=\psi_0 f_{i,j}\quad\text{at } \tau=0,\tag{31}$$

$$\tilde{\bar{\Theta}}_{m,n}=f_{m,n}^*\quad\text{at } \tau=0\tag{32}$$

and f, f^*, A, B, C and D represent the integral coefficients obtained throughout the integral transformation and are given by

$$f_{i,j}=\int_0^1\Phi_i(X)\,\mathrm{d}X\int_0^H\Phi_j^*(Z)\,\mathrm{d}Z,\tag{33}$$

$$f_{m,n}^*=\int_0^1(\theta_0-X)\Gamma_m(X)\,\mathrm{d}X\int_0^H\Gamma_n^*(Z)\,\mathrm{d}Z,\tag{34}$$

$$A_{i,j,m,n}=\int_0^1\Phi_i(X)\Gamma_m(X)\,\mathrm{d}X\int_0^H\Phi_j^*(Z)\frac{\mathrm{d}\Gamma_n^*(Z)}{\mathrm{d}Z}\,\mathrm{d}Z,\tag{35}$$

$$B_{m,n,i,j}=\int_0^1\Gamma_m(X)\Phi_i(X)\,\mathrm{d}X\int_0^H\Gamma_n^*(Z)\frac{\mathrm{d}\Phi_j^*(Z)}{\mathrm{d}Z}\,\mathrm{d}Z,\tag{36}$$

$$C_{m,n,i,j,o,p}=\int_0^1\Gamma_m(X)\Phi_i(X)\frac{\mathrm{d}\Gamma_o(X)}{\mathrm{d}X}\,\mathrm{d}X\times\int_0^H\Gamma_n^*(Z)\frac{\mathrm{d}\Phi_j^*(Z)}{\mathrm{d}Z}\Gamma_p^*(Z)\,\mathrm{d}Z,\tag{37}$$

$$D_{m,n,i,j,o,p}=\int_0^1\Gamma_m(X)\frac{\mathrm{d}\Phi_i(X)}{\mathrm{d}X}\Gamma_o(X)\mathrm{d}X\times\int_0^H\Gamma_n^*(Z)\Phi_j^*(Z)\frac{\mathrm{d}\Gamma_p^*(Z)}{\mathrm{d}Z}\,\mathrm{d}Z.\tag{38}$$

System (29)–(32) defines the set of coupled nonlinear ODEs to be numerically solved for the transformed potentials, at any user requested value of dimensionless time. Using the inversion formulae (25) and (28) with a suitable reordering scheme [6,7], one can obtain the single series expansions shown below:

$$\begin{aligned}\psi(X,Z,\tau)&=\sum_{i=1}^{\infty}\sum_{j=1}^{\infty}\Phi_i(X)\Phi_j^*(Z)\tilde{\bar{\psi}}_{i,j}(\tau)\\&=\sum_{k=1}^{N}\Phi_{i(k)}(X)\Phi_{j(k)}^*(Z)\tilde{\bar{\psi}}_{i(k),j(k)}(\tau),\end{aligned}\tag{39}$$

$$\begin{aligned}\theta(X,Z,\tau)&=X+\sum_{m=1}^{\infty}\sum_{n=0}^{\infty}\Gamma_m(X)\Gamma_n^*(Z)\tilde{\bar{\Theta}}_{m,n}(\tau)\\&=X+\sum_{l=1}^{M}\Gamma_{m(l)}(X)\Gamma_{n(l)}^*(Z)\tilde{\bar{\Theta}}_{m(k),n(k)}(\tau),\end{aligned}\tag{40}$$

where $\Phi_i(X)$, $\Phi_j^*(Z)$, $\Gamma_m(X)$ and $\Gamma_n^*(Z)$ are the eigenfunctions obtained from the eigenproblem (11)–(22) used as the basis for the integral transformation.

Local Nusselt number results used in this analysis were obtained from

$$Nu(Z,\tau)=\left.\frac{\partial\theta}{\partial X}\right|_{X=1}\tag{41}$$

and average Nusselt number results were obtained from

$$Nu_{\mathrm{av}}(\tau)=\frac{1}{H}\int_0^H\left.\frac{\partial\theta}{\partial X}\right|_{X=1}\mathrm{d}Z.\tag{42}$$

By properly truncating the expansions in Eqs. (29) and (30) or (25) and (28), one can for instance generate the system of three equations below:

$$\frac{\mathrm{d}\tilde{\bar{\psi}}_{1,1}(\tau)}{\mathrm{d}\tau}=-\chi\left(\frac{RaH}{(H^2+1)\pi}\tilde{\bar{\Theta}}_{1,1}(\tau)+\tilde{\bar{\psi}}_{1,1}(\tau)\right),\tag{43}$$

$$\begin{aligned}\frac{\mathrm{d}\tilde{\bar{\Theta}}_{1,1}(\tau)}{\mathrm{d}\tau}=&-\left(1+\frac{1}{H^2}\right)\pi^2\tilde{\bar{\Theta}}_{1,1}(\tau)\\&-\left(\frac{\pi}{H}-\frac{\sqrt{2}\pi^2}{H^{3/2}}\tilde{\bar{\Theta}}_{2,0}(\tau)\right)\tilde{\bar{\psi}}_{1,1}(\tau),\end{aligned}\tag{44}$$

$$\frac{d\tilde{\tilde{\Theta}}_{2,0}(\tau)}{d\tau} = -4\pi^2\tilde{\tilde{\Theta}}_{2,0}(\tau) - \frac{\sqrt{2}\pi^2}{H^{3/2}}\tilde{\tilde{\Theta}}_{1,1}(\tau)\tilde{\tilde{\psi}}_{1,1}(\tau), \tag{45}$$

where the respective initial conditions are

$$\tilde{\tilde{\psi}}_{1,1}(0) = \frac{8\sqrt{H}}{\pi^2}\psi_0, \tag{46}$$

$$\tilde{\tilde{\Theta}}_{1,1}(0) = 0, \tag{47}$$

$$\tilde{\tilde{\Theta}}_{2,0}(0) = \frac{1}{\pi}\sqrt{\frac{H}{2}}. \tag{48}$$

The steady-state solutions of Eqs. (43)–(45) are

$$\tilde{\tilde{\psi}}_{1,1}(\infty) = 0, \quad \tilde{\tilde{\Theta}}_{1,1}(\infty) = 0, \quad \tilde{\tilde{\Theta}}_{2,0}(\infty) = 0, \tag{49}$$

$$\begin{aligned}
\tilde{\tilde{\psi}}_{1,1}(\infty) &= \frac{1}{\pi}\sqrt{\frac{2H^3Ra}{1+H^2} - 2H(1+H^2)\pi^2},\\
\tilde{\tilde{\Theta}}_{1,1}(\infty) &= -\frac{1+H^2}{HRa}\sqrt{\frac{2H^3Ra}{1+H^2} - 2H(1+H^2)\pi^2},\\
\tilde{\tilde{\Theta}}_{2,0}(\infty) &= \frac{H^2Ra - (1+H^2)^2\pi^2}{\sqrt{2}H^{3/2}\pi Ra},
\end{aligned} \tag{50}$$

$$\begin{aligned}
\tilde{\tilde{\psi}}_{1,1}(\infty) &= -\frac{1}{\pi}\sqrt{\frac{2H^3Ra}{1+H^2} - 2H(1+H^2)\pi^2},\\
\tilde{\tilde{\Theta}}_{1,1}(\infty) &= \frac{1+H^2}{HRa}\sqrt{\frac{2H^3Ra}{1+H^2} - 2H(1+H^2)\pi^2},\\
\tilde{\tilde{\Theta}}_{2,0}(\infty) &= \frac{H^2Ra - (1+H^2)^2\pi^2}{\sqrt{2}H^{3/2}\pi Ra},
\end{aligned} \tag{51}$$

where Eq. (49) represents the conduction steady-state solution and Eqs. (50) and (51) represent two possible convection steady-state solutions.

Eqs. (43)–(45) can be transformed into the so-called Lorenz equations by using one of the convection fixed point solutions (50) and (51) to re-scale the transformed potentials and then re-scale the time variable as well, to obtain

$$\frac{dY_1(t)}{dt} = p_1(-Y_1(t) + Y_2(t)), \tag{52}$$

$$\frac{dY_2(t)}{dt} = -Y_2(t) + Y_1(t)(p_2 + (1-p_2)Y_3(t)), \tag{53}$$

$$\frac{dY_3(t)}{dt} = 4p_3(Y_1(t)Y_2(t) - Y_3(t)), \tag{54}$$

where the constants and the time variable from the above equations are defined as

$$\begin{aligned}
p_1 &= \frac{\chi H^2}{(1+H^2)\pi^2}, \quad p_2 = \frac{H^2Ra}{(1+H^2)^2\pi^2},\\
p_3 &= \frac{H^2}{1+H^2} \quad \text{and} \quad \tau = \frac{H^2}{(1+H^2)\pi^2}t.
\end{aligned} \tag{55}$$

Applying the same scaling to the initial conditions (46)–(48) we find

$$Y_1(0) = \frac{4\sqrt{2}\psi_0}{\pi^2\sqrt{(1+H^2)(p_2-1)}}, \tag{56}$$

$$Y_2(0) = 0, \tag{57}$$

$$Y_3(0) = \frac{p_2}{p_2-1}. \tag{58}$$

The initial conditions above are those to be used with Lorenz equations whenever they are derived from a problem formulation such as in (29) and (30), in order to maintain the validity of the problem physics. Other initial conditions have been used [3,14,15] in order to demonstrate the solution behavior around the fixed points.

4. Linear stability analysis (LSA)

The nature of the dynamics about the fixed points (49)–(51), of the dissipative system (43)–(45) (or, in a more general form, Eqs. (29) and (30)), is then investigated. When such systems can be re-written in the more compact form

$$\frac{d\mathbf{X}}{dt} = F(\mathbf{X}, \lambda), \tag{59}$$

where $\mathbf{X}$ represents the potentials of the system and λ its control parameters, their equilibrium points are defined by

$$F(\mathbf{X}_s, \lambda) = 0. \tag{60}$$

The stability matrix is established by evaluating the Jacobian J,

$$J_{i,j} = \left.\frac{\partial F_i}{\partial X_j}\right|_{\mathbf{X}_s} \tag{61}$$

at the fixed point of interest $\mathbf{X}_s$.

Based on this matrix, one can use the *principle of linearized stability* [11] to compare the stability properties of the fully nonlinear problem and the auxiliary linearized one in which higher-order terms are omitted. Considering ω the eigenvalues of the stability matrix, we can summarize the basic ideas of this principle on the two statements below:

1. If $Re\|\omega\| < 0$, the reference state $\mathbf{X}_s$ is asymptotically stable.
   If $Re\|\omega\| > 0$, the reference state $\mathbf{X}_s$ is unstable.
2. If the transversality condition is satisfied ($dRe\|\omega\|/d\lambda|_{\lambda=\lambda_0} \neq 0$; $\lambda_0 \equiv$ critical parameter) and ω is an eigenvalue of odd multiplicity, one can say that:
   - After bifurcation, the solutions will be stationary if $\mathrm{Im}\|\omega\| = 0$,
   - After bifurcation, the solutions will be periodic if $\mathrm{Im}\|\omega\| \neq 0$.

These statements set up a quantitative criterion to establish if the steady-state solutions are stable or not and to distinguish two important critical parameters, the Rayleigh numbers at onset of convection and at onset of chaos. (or, more precisely, periodic or non-periodic regimer)

The results obtained from this linearized analysis are compared with those generated from a direct numerical simulation of the full nonlinear system, using the well-established numerical algorithms built-in function NDSolve of the *Mathematica* software system [10] to solve the Ntth order truncated system formed by (29) and (30) and initial conditions (31) and (32).

5. Results and discussion

All numerical solutions were obtained using the same initial conditions, which were selected as $\psi_0 = 0.1$, $\theta_0 = 0.5$ and for $\chi = 1000$ [16]. Eqs. (43)–(45) were used instead of the Lorenz equations form (52)–(54) to make it easier to compare their results with those from higher dimensional systems generated from Eqs. (29) and (30). Critical Rayleigh numbers and Nusselt numbers dependence on the aspect ratio, obtained from higher dimensional systems, are then investigated.

Using the system of three Eqs. (43)–(45), the LSA returns

$$Ra'_{\mathrm{cond1}} = \frac{Ra_{\mathrm{cond}}}{\pi^2} = \frac{(1+H^2)^2}{H^2}, \tag{62}$$

where Ra_{cond} is the Rayleigh number at onset of convection, as a function of the cavity aspect ratio. However, when we increase the order of the truncated system to 21 equations, the LSA then returns

$$Ra'_{\mathrm{cond2}} = \frac{(9+H^2)^2}{9H^2}. \tag{63}$$

Using a system of 21 equations, the obtained Rayleigh number at onset of convection (Ra_{cond}) goes through a sudden change in its behavior as a function of the aspect ratio, H, which does not occur to the system of three equations, passing through a minimum and then increasing again. The comparison of Eqs. (62) and (63) with these numerical results generated is presented in Fig. 2, where one may see a good agreement between results for the linear and nonlinear approaches.

When the number of equations numerically solved is gradually increased to 136, other peaks in the Ra_{cond} versus H behavior can be observed. The comparison of the obtained numerical results is presented in Fig. 3, where systems with $Nt = 3,\ 21,\ 55,\ 105$ and 136 equations are shown and demonstrate the numerical convergence of the critical parameter solution.

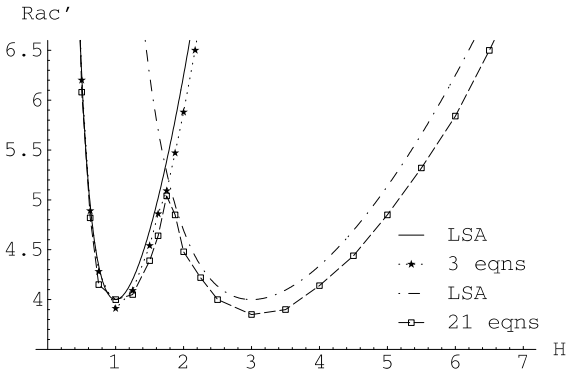

Fig. 2. Ra'_{cond} versus H: linear stability analysis and numerical results.

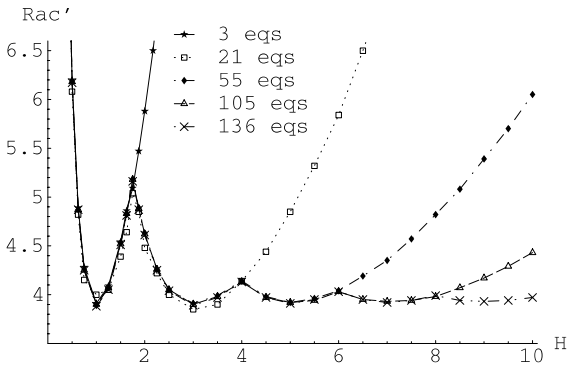

Fig. 3. Ra'_{cond} versus H: numerical results for 3, 21, 55, 105 and 136 equations.

The peaks that one can observe in Figs. 2 and Fig. 3 appear due to the transition of the pattern structure from 1 to 3 cells, from 3 to 5 cells, ..., from n to $n+2$, up to the parallel plate cell structure at $H \to \infty$. Stream function and temperature isolines right before and after the transition points are shown in Fig. 4, where the pattern modification from 1 to 3 cells appears in Fig. 4(a), from 3 to 5 cells in Fig. 4(b), and from 5 to 7 in Fig. 4(c). In this way, formula (62) provides the critical Rayleigh number when the cavity presents a one-roll cell structure, in the same way as formula (63) provides the value of this parameter when the cavity presents a three-roll cell structure. The difference between the two formulae relies on the number of rolls within the structure, allowing the generalization of Eqs. (62) and (63) valid for any number of rolls as

$$Ra'_{\mathrm{cond}} \to \frac{(1+H^2)^2}{H^2} \to \frac{(9+H^2)^2}{9H^2} \to \cdots \to \frac{(n^2+H^2)^2}{n^2H^2}, \tag{64}$$

where n is the number of rolls in the cavity cell structure.

Expression (64) is similar to the one presented by Caltagirone [13] and through it one may find the various

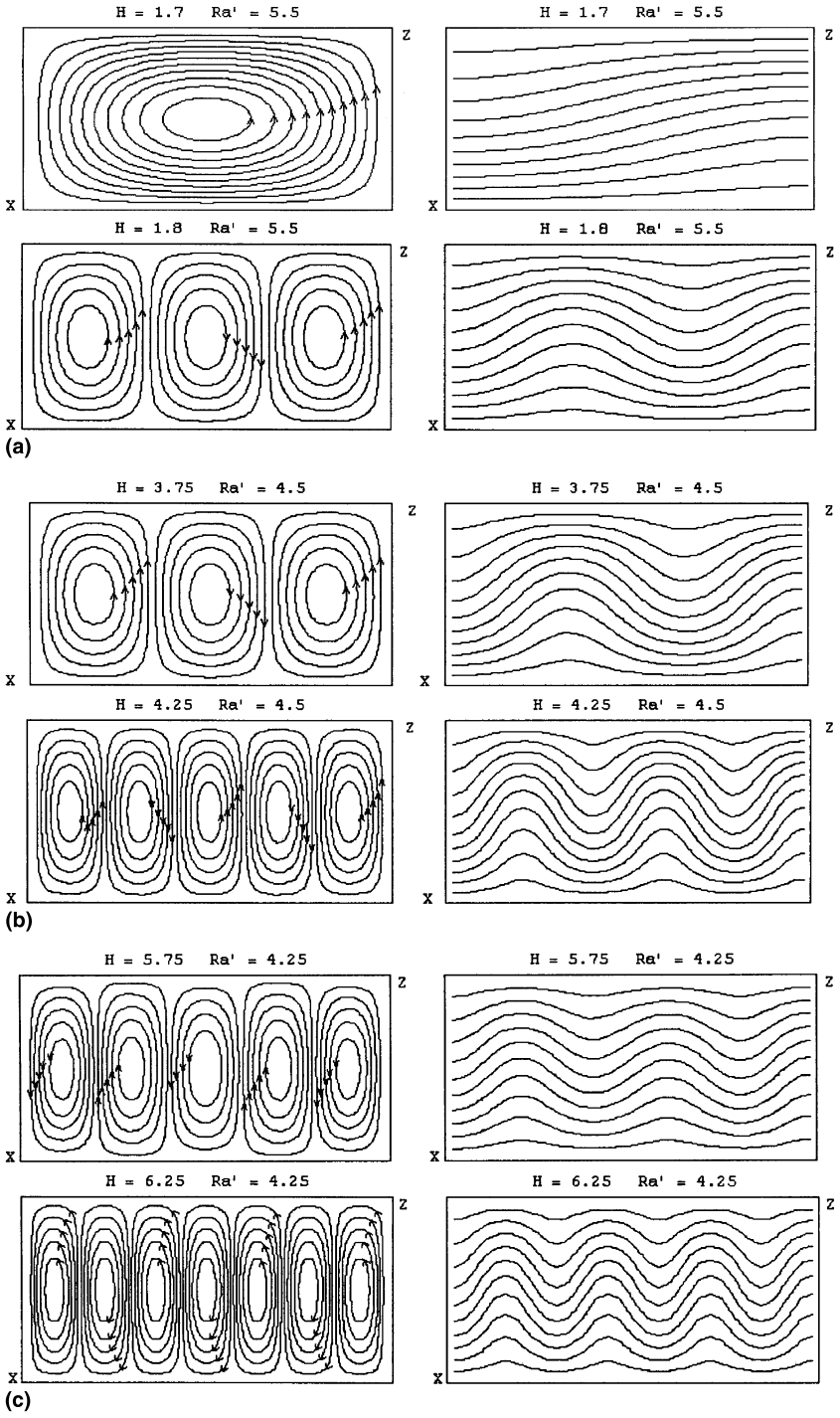

Fig. 4. Stream function and temperature transition of the cell structures: (a) 1–3 cells, (b) 3–5 cells and (c) 5–7 cells.

values of the aspect ratio and Rayleigh number at onset of convection when the transitions occur. These results are presented in Table 1, where numerical and analytical solutions are compared, showing a good agreement.

Knowing that the number of cells in each structure is odd, one may find the values of H when the singularities appear by equating Eq. (64) for an n cell structure to Eq. (64) for an $n+2$ cell structure. Doing so, one may find

Table 1
Comparison of analytical and numerical results of the cell transition points

n	$1 \rightarrow 3$	$3 \rightarrow 5$	$5 \rightarrow 7$	$7 \rightarrow 9$
$H_{\text{analytical}}$	$\sqrt{3}$ (1.73)[a]	$\sqrt{15}$ (3.87)	$\sqrt{35}$ (5.92)	$3\sqrt{7}$ (7.94)
$H_{\text{numerical}}$	1.75	3.88	6.00	8.06
$Ra_{\text{cond,analytical}}$	16/3 (5.33)[a]	64/15 (4.27)	144/35 (4.11)	256/63 (4.06)
$Ra_{\text{cond,numerical}}$	5.19	4.18	4.04	3.96

[a] Rounded values.

the formula that generated the values that appear in Table 1,

$$H_{\text{sing}} = (n^2(n+2)^2)^{1/4} \quad \text{for } n = 1(1 \rightarrow 3), 3(3 \rightarrow 5), 5(5 \rightarrow 7), \ldots \tag{65}$$

and in the same way, the formula used to find the values of Ra'_{cond} at the singularity points presented in Table 1 is given by

$$Ra'_{\text{cond,sing}} = \frac{4(n+1)^2}{n(n+2)} \quad \text{for } n = 1(1 \rightarrow 3), 3(3 \rightarrow 5), 5(5 \rightarrow 7), \ldots \tag{66}$$

Using the values provided by Eqs. (65) and (66), the numerical results obtained from the system of 136 equations can be compared with Eq. (64) in Fig. 5, showing a very good agreement between the LSA and the GITT hybrid solution of the full nonlinear system.

Another group of points can be found from expression (64), associated with the cell symmetry. At the values of H and Ra'_{cond} given by Eq. (64), Nusselt number has its lowest local value. However, at the points of minimum energy dissipation, the perturbation introduced by the cell breakdown is minimum, causing the cell structure to be symmetric. There is more than one point of minimum due to the cell structure modification caused by the geometry variation and some of the points of symmetry can be observed in Fig. 6. These points can be found by equating the derivative of Eq. (64) with respect to H to 0, which gives $H = n$ as a solution ($n = 1, 3, 5, \ldots$). Using this solution at Eq. (64), one may find $Ra_{\text{cond}} = 4\pi^2$ [3,13]. Nevertheless, these same points, when obtained by direct numerical simulation are lower than $4\pi^2$, as one may see in Fig. 5. Also, when $H \rightarrow \infty$ we have that $n \rightarrow H$, which makes it possible to find the parallel plate Rayleigh number at onset of convection from Eq. (66), $4\pi^2$.

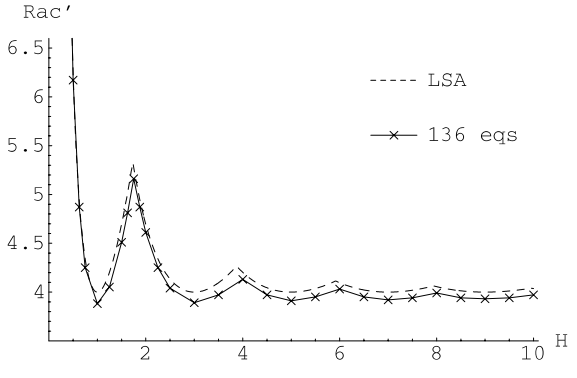

Fig. 5. Ra'_{cond} versus H: generalized analytical solution and numerical results.

Fig. 7 presents the steady-state average Nusselt number variation with aspect ratio for $Ra = 50,\ 55$ and 100, where the influence of the aspect ratio on the cell pattern transition can be observed. One may see that for $Ra = 50$, Nu_{av} re-enters the conduction region ($Nu_{\text{av}} = 1$) between $0 < H < 0.6$ and $1.6 < H < 1.8$. For $Ra = 55$, average Nusselt numbers are out of the conduction region for $H > 0.6$. This figure also shows the influence of the Rayleigh number on the cell pattern transition since the peaks occur at lower aspect ratio values for $Ra = 100$ in comparison to $Ra = 55$. This influence can be better observed in Fig. 8, where steady-state local Nusselt numbers of a square cavity are presented. For $Ra = 50,\ 100$ and 200 there is a one-roll cell structure, but at $Ra = 300$ a three-roll cell structure appears.

Following the LSA procedure, but now using the convection steady-state solution as the reference state, the Rayleigh number at onset of chaos may be found. Using Lorenz system one may find the following expression:

$$Ra_{\text{conv}} = \frac{(1+H^2)\chi((3+7H^2)\pi^2 + H^2\chi)}{H^2\chi - (1+5H^2)\pi^2} \tag{67}$$

which is equivalent to the one found by Vadasz and Olek [3].

The comparison of Eq. (67) with numerical results for $\chi = 1000$ and 10 000 is shown in Fig. 9. Despite the fact that Eq. (67) has been derived from a system of three equations, it allows a qualitative interpretation of this critical parameter. The time derivative coefficient from the momentum equation, χ, has a significant influence on the Rayleigh number at onset of chaos. The critical parameter expression relative to the classical Darcy model can be obtained by taking $\chi \rightarrow \infty$,

$$Ra_{\text{conv}} = (1+H^2)\chi, \tag{68}$$

which shows that the classical Darcy model without transient term in the momentum equations, eliminates the chaotic region by extending the convection region to infinity.

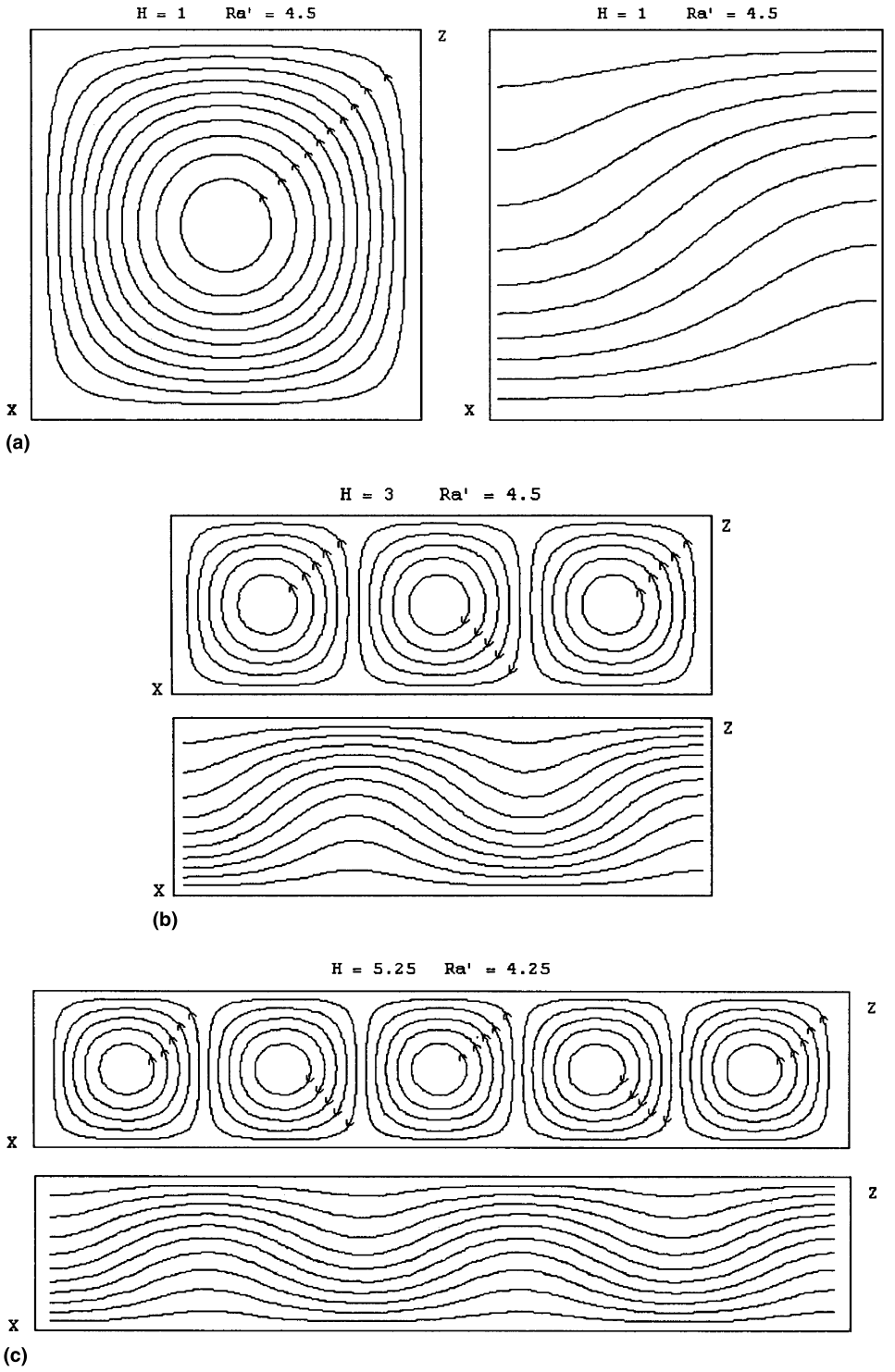

Fig. 6. Stream function and temperature isolines at local minima: (a) $H = 1$, (b) $H = 3$ and (c) $H = 5.25$.

The analysis of the Rayleigh number at onset of chaos through the full nonlinear system solution proved to be much more computationally involved than for the case at onset of convection, since much larger truncation orders were required for full convergence to be obtained by the GITT algorithm. Fig. 10 shows the behavior of

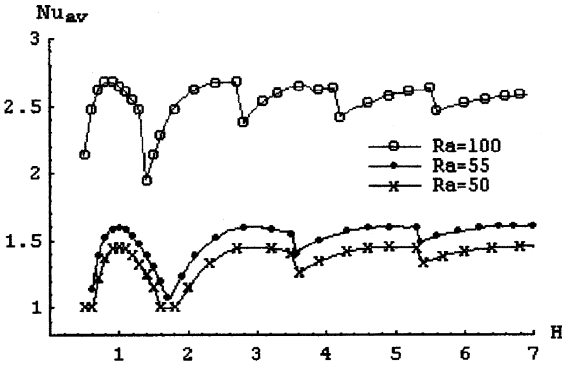

Fig. 7. Steady-state average Nusselt number against aspect ratio: $Ra = 50,\ 55$ and 100.

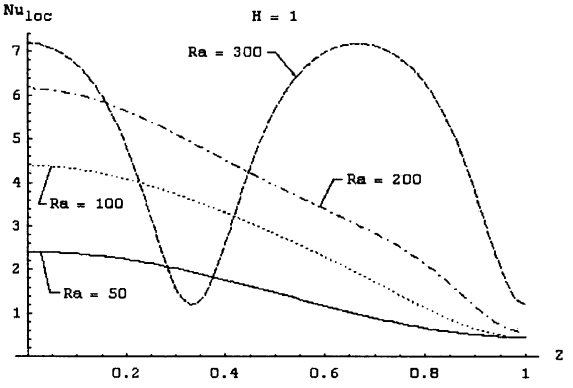

Fig. 8. Square cavity steady-state local Nusselt number: $Ra = 50,\ 100,\ 200$ and 300.

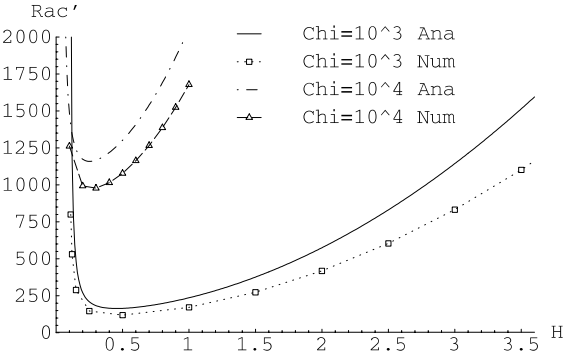

Fig. 9. Ra'_{conv} versus H: $\chi = 1000$ and 10 000.

Ra'_{conv}, for $H = 1$ and $\chi = 100$ when the total number of equations $Nt = N + M$ used in the direct numerical simulation is increased. LSA loses adherence when Nt is increased, which was expected since the nonlinear terms in the system are increased in number and importance, and presentation of such results is here avoided.

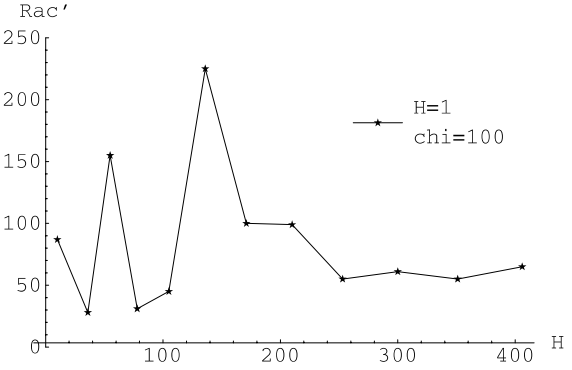

Fig. 10. Ra'_{conv} versus Nt: $\chi = 100$ and $H = 1$.

6. Conclusions

Cell pattern transition and aspect ratio govern the behavior of the Rayleigh number at onset of convection. Nusselt numbers, as well as the cell transition points, are determined by Rayleigh number and aspect ratio. The structure change from n to $n + 2$ ($n = 1, 3, 5, \ldots$) cells causes a sharp variation in both Nusselt and Rayleigh number at onset of convection.

The importance of the time derivative term, usually excluded from the Darcy model, was shown to be vital for the proper understanding of natural convection in cavities heated from below. Even though the critical Rayleigh number at onset of convection shows no dependence on χ, the parameter gauging the transient behavior in the system, the critical Rayleigh number at onset of chaos qualitative behavior is clearly dependent on the modeling of the flow history, which is not properly taken into account in the classic Darcy model.

The GITT proved to be quite useful in this analysis since it was capable of capturing the Rayleigh number influence on the cell transition point, which does not necessarily occur when purely numerical methods are employed [17]. In order to reduce convergence oscillations in the results for the Rayleigh number at onset of chaos, and thus reduce computational costs, GITT must be used together with recently advanced optimization schemes such as local-instantaneous filtering and dynamical reordering [6,7].

The symbolic manipulation allowed by the *Mathematiaca* software system, besides the fact that it fits perfectly with analytic-based approaches such as the present integral transform method [6], improves the reliability in the analytical steps needed in the stability analysis.

References

[1] S. Kakaç, B. Kilkiş, F.A. Kulacki, F. Arinç (Eds.), Convective Heat and Mass Transfer in Porous Media,

Kluwer Academic Publishers, Dordrecht, The Netherlands, 1990.
[2] M. Kaviany, Principles of Heat Transfer in Porous Media, second ed., Springer, New York, 1995.
[3] P. Vadasz, S. Olek, Transitions and chaos for free convection in a rotating porous layer, Int. J. Heat Mass Transfer 4111 (1998) 1417–1435.
[4] L.S.de B. Alves, R.M. Cotta, Transient natural convection inside porous cavities: hybrid numerical–analytical solution and mixed symbolic–numerical computation, Numer. Heat Transfer A 481 (2000) 89–110.
[5] R.M. Cotta, Integral Transforms in Computational Heat and Fluid Flow, CRC Press, Boca Raton, FL, 1993.
[6] R.M. Cotta, M.D. Mikhailov, Heat Conduction Lumped Analysis, Integral Transforms, Symbolic Computation, Wiley, UK, 1997.
[7] R.M. Cotta (Ed.), The Integral Transform Method in Thermal and Fluids Science and Engineering, Begell House, New York, 1998.
[8] M.D. Mikhailov, M.N. Özisik, Unified Analysis and Solutions of Heat and Mass Diffusion, Wiley, New York, 1984.
[9] S. Wolfram, Mathematica: A System for Doing Mathematics by Computer, Addison-Wesley, Redwood City, CA, 1991.
[10] S. Wolfram, The Mathematica Book, fourth ed., Wolfram Media, Cambridge, 1999.
[11] G. Nicolis, Introduction to NonLinear Science, Cambridge University Press, UK, 1995.
[12] R.N. Horne, M.J. O'Sullivan, Oscillatory convection in a porous medium heated from below, J. Fluid Mech. 66 (1974) 339–352.
[13] J.P. Caltagirone, Thermoconvective instabilities in a horizontal porous layer, J. Fluid Mech. 72 (1975) 269–287.
[14] P. Vadasz, Subcritical transitions to chaos and hysteresis in a fluid layer heated from below, Int. J. Heat Mass Transfer 43 (2000) 705–724.
[15] P. Vadasz, On the homoclinic orbit for the convection in a fluid layer heated from below, Int. J. Heat Mass Transfer 42 (1999) 3557–3561.
[16] L.S.de B. Alves, H.L. Neto, R.M. Cotta, Parametric analysis of the streamfunction time derivative in the Darcy-flow model for transient natural convection, in: 2nd International Conference on Computational Heat and Mass Transfer, CHMT-2001, Rio de Janeiro, Brazil, October 2001 (CD-ROM).
[17] J.R. Figueiredo, J. Llagostera, Comparative study of the unified finite approach exponential-type scheme unifaces and its application to natural convection in a porous cavity, Numer. Heat Transfer B 35 (1999) 347–367.